Computational Mechanics 28 (2002) 351–364 © Springer-Verlag 2002
DOI 10.1007/s00466-002-0299-x

Probabilistic fracture mechanics by Galerkin meshless methods – part I: rates of stress intensity factors

B. N. Rao, S. Rahman

Abstract This is the first in a series of two papers generated from a study on probabilistic meshless analysis of cracks. In this paper (Part I), a Galerkin-based meshless method is presented for predicting first-order derivatives of stress-intensity factors with respect to the crack size in a linear-elastic structure containing a single crack. The method involves meshless discretization of cracked structure, domain integral representation of the fracture integral parameter, and sensitivity analysis in conjunction with a virtual crack extension technique. Unlike existing finite-element methods, the proposed method does not require any second-order variation of the stiffness matrix to predict first-order sensitivities, and is, consequently, simpler than existing methods. The method developed herein can also be extended to obtain higher-order derivatives if desired. Several numerical examples related to mode-I and mixed-mode problems are presented to illustrate the proposed method. The results show that first-order derivatives of stress-intensity factors using the proposed method agree very well with reference solutions obtained from either analytical (mode I) or finite-difference (mixed mode) methods for the structural and crack geometries considered in this study. For mixed-mode problems, the maximum difference between the results of proposed method and finite-difference method is less than 7%. Since the rates of stress-intensity factors are calculated analytically, the subsequent fracture reliability analysis can be performed efficiently and accurately.

Keywords Element-free Galerkin method, Virtual crack extension, Stress-intensity factor, Rates of stress-intensity factor, Interaction integral, Linear-eleastic fracture mechanics

1 Introduction

In recent years, various Galerkin-based meshless methods have been developed or investigated to solve fracture-mechanics problems without the use of a structured grid [1–7]. These meshless methods employ moving least-squares (MLS) approximation of a function that permits the resultant shape functions to be constructed entirely in terms of arbitrarily placed nodes. Since no element connectivity data is required, the burdensome meshing or remeshing characteristic of finite element methods (FEMs) is avoided. However, most development in meshless methods to date has been focused on deterministic problems. Research in probabilistic meshless analysis has not been widespread and is only currently gaining attention. Recently, Rahman and Rao [8, 9] and Rahman and Xu [10] developed stochastic meshless methods for solving linear-elastic problems that involve spatially varying random material properties. The methods provide accurate estimates of second-moment characteristics of structural response and reliability [8–10]. However, the aforementioned methods do not include fracture-mechanics theory and are, therefore, not applicable to probabilistic analysis of cracks. Hence, there is considerable interest in developing stochastic meshless methods that are capable of treating uncertainties in loads, material properties, and crack geometry and predicting probabilistic fracture response and reliability of cracked structures. Such an undertaking represents a qualitatively new theoretical development, employing meshless methods to account for probabilistic aspects of fracture processes. To the best knowledge of the authors, no meshless models for probabilistic fracture-mechanics (PFM) analysis exist in the current literature.

In PFM, the derivatives of the stress-intensity factor (SIF) or integral parameters are often required to predict the probability of fracture initiation and/or instability in cracked structures. First- and second-order reliability methods [11], frequently used in PFM [12–18], require the gradient and/or Hessian of the performance function with respect to random parameters. In linear-elastic fracture mechanics (LEFM), the performance function is built on SIFs. Hence, both first- and/or second-order derivatives of SIF are needed in PFM. The calculation of these derivatives with respect to load and material parameters, which constitutes size-sensitivity analysis, is not unduly difficult. However, the evaluation of response derivatives with respect to crack size is a challenging task, since shape sensitivity analysis is required. Using a brute-force type finite-difference method to calculate shape sensitivities is often computationally expensive, in that numerous repetitions of deterministic meshless analysis may be required for a complete reliability analysis. Furthermore, if the finite-difference perturbations are too large relative to

Received 20 February 2001 / Accepted 19 December 2001

B. N. Rao, S. Rahman (✉)
College of Engineering, The University of Iowa,
Iowa City, IA 52242, USA
e-mail: rahman@engineering.uiowa.edu

The authors would like to acknowledge the financial support of the U.S. National Science Foundation (NSF) under Award No. CMS-9900196. The NSF program director is Dr. Ken Chong.

meshless discretization, the approximations can be inaccurate, whereas if the perturbations are too small, numerical truncation errors may become significant. Consequently, analytical methods based on virtual crack extension [19–24] and continuum shape sensitivity theory [25–30] have emerged. In 1988, Lin and Abel [19] introduced a virtual crack extension technique that employs a variational formulation and a FEM to calculate the first-order derivative of mode-I SIF for a structure containing a single crack. This method maintains all of the advantages of similar virtual crack extension techniques introduced by deLorenzi [20, 21], Haber and Koh [22], and Barbero and Reddy [23], but adds a capability to calculate the derivatives of the SIF. Subsequently, Hwang et al. [24] generalized this method to calculate both first- and second-order derivatives for structures with multiple crack systems, axisymmetric stress states, and crack-face and thermal loading. However, this method requires mesh perturbation – a fundamental requirement of all virtual crack extension techniques. For second-order derivatives, the number of elements affected by mesh perturbation surrounding the crack tip has a significant effect on solution accuracy [24]. Recently, Feijóo et al. [25] applied the concepts of continuum shape sensitivity theory [26] to calculate the first-order derivative of the potential energy. Since the energy release rate (ERR) is the first-order derivative of potential energy, the ERR or SIF can be calculated using this approach, without any mesh perturbation. Later, Taroco [27] extended this approach to formulate the second-order sensitivity of potential energy to predict the first-order derivative of the ERR. However, this presents a formidable task, since it involves calculation of second-order stress and strain sensitivities. To overcome this difficulty, Chen et al. [28, 29] invoked the domain integral representation of the *J*-integral and used the material derivative concept of continuum mechanics to obtain first-order sensitivity of the *J*-integral for linear-elastic cracked structures. Since this method requires only the first-order sensitivity of a displacement field, it is simpler and more efficient than existing methods. Recently, Chen et al. [30] extended their continuum shape sensitivity method for mixed-mode loading conditions. All of these methods, however, have been developed only in conjunction with FEM. Consequently, there is a need to develop meshless-based sensitivity equations for SIFs so that subsequent stochastic meshless analysis of cracks can be efficiently performed.

This is the first in a series of two papers generated from a study on probabilistic fracture mechanics applying Galerkin-based meshless methods. In this paper (Part I), a virtual crack extension technique in conjunction with an element-free Galerkin method (EFGM) is presented for calculating first-order sensitivities of SIFs in two-dimensional, homogeneous, isotropic, linear-elastic cracked structures. The proposed method involves meshless discretization of cracked structures, domain integral representation of the fracture integral parameter, and sensitivity analysis in conjunction with a virtual crack extension technique. Since the fracture response parameters are represented by domain integration, only the first-order sensitivity of displacement field is required. Numerical examples based on mode-I and mixed-mode problems are presented to illustrate the proposed method. The probabilistic meshless analysis of cracks using first-order sensitivities of SIFs is described in the companion paper (Part II) [31].

2 Element-free Galerkin method

2.1 Variational principle and discretization

Consider a two-dimensional structure with a rectilinear crack of length $2a$ and orientation γ, subjected to external loads, $S_1, S_2, \ldots, S_M$, as shown in Fig. 1. The meshless discretization of this cracked structure is shown in Fig. 2. For small displacements in homogeneous, isotropic, linear-elastic solids, the variational or weak form of equilibrium equations and boundary conditions are

$$\int_{\Omega} \boldsymbol{\sigma}^{\mathrm{T}} \delta \boldsymbol{\epsilon} \, \mathrm{d}\Omega - \int_{\Omega} \mathbf{b}^{\mathrm{T}} \delta \mathbf{u} \, \mathrm{d}\Omega - \int_{\Gamma_t} \bar{\mathbf{t}}^{\mathrm{T}} \delta \mathbf{u} \, \mathrm{d}\Gamma + \delta W_u = 0 \tag{1}$$

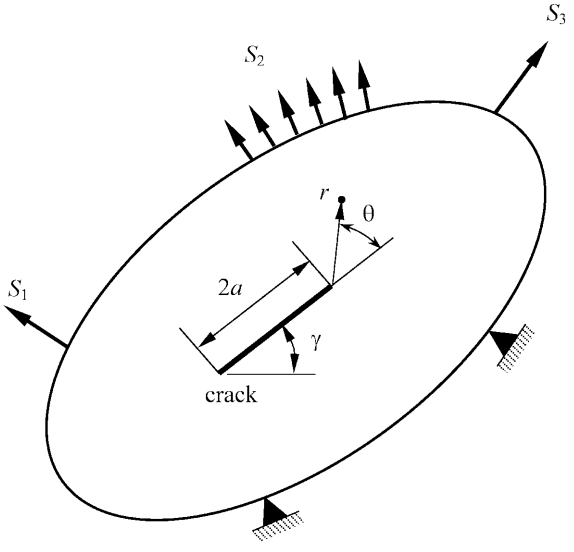

Fig. 1. A cracked structure under mixed-mode loading

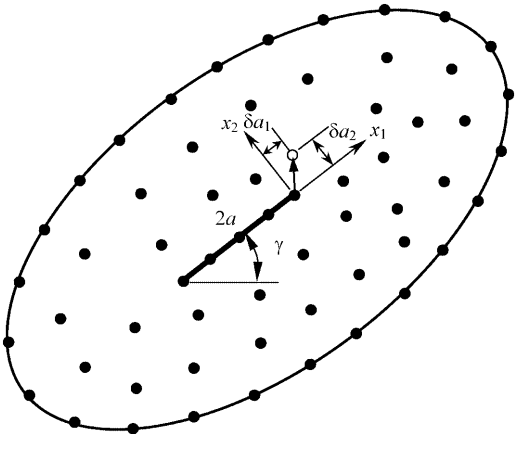

Fig. 2. Meshless discretization and virtual crack extension

$$\delta W_u = \sum_{x_J \in \Gamma_u} \delta \mathbf{f}^{\mathrm{T}}(\mathbf{x}_J)[\mathbf{u}(\mathbf{x}_J) - \bar{\mathbf{u}}(\mathbf{x}_J)] + \mathbf{f}^{\mathrm{T}}(\mathbf{x}_J)\delta \mathbf{u}(\mathbf{x}_J) \tag{2}$$

where $\mathbf{x} = \{x_1, x_2\}^{\mathrm{T}} \in \Re^2$ is any point in the domain $\Omega \subseteq \Re^2$, $\mathbf{u} = \{u_1, u_2\}^{\mathrm{T}} \in \Re^2$ is the displacement vector, $\boldsymbol{\sigma} = \{\sigma_1, \sigma_2, \sigma_{12}\}^{\mathrm{T}} \in \Re^3$ is the stress vector, $\boldsymbol{\epsilon} = \{\varepsilon_1, \varepsilon_2, 2\varepsilon_{12}\}^{\mathrm{T}} \in \Re^3$ is the strain vector, $\mathbf{b}$ is the body force vector, $\bar{\mathbf{t}}$ and $\bar{\mathbf{u}}$ are the vectors of prescribed surface tractions and displacements, respectively, $\mathbf{f}^{\mathrm{T}}(\mathbf{x}_J)$ is the vector of reaction forces at the constrained node $J \in \Gamma_u$, Γ_t and Γ_u are the portions of boundary Γ where tractions and displacements are respectively prescribed, and δ is the variation operator. Consider a single boundary constraint, $\bar{u}_i(\mathbf{x}_J) = g_i(\mathbf{x}_J)$ applied at node J in the direction of the x_i coordinate. The variational form given by Eqs. (1) and (2) can then be expressed by [1]

$$\int_{\Omega} \boldsymbol{\sigma}^{\mathrm{T}} \delta \boldsymbol{\epsilon}\, \mathrm{d}\Omega + f_i(\mathbf{x}_J)\delta u_i(\mathbf{x}_J) = \int_{\Omega} \mathbf{b}^{\mathrm{T}} \delta \mathbf{u}\, \mathrm{d}\Omega + \int_{\Gamma_t} \bar{\mathbf{t}}^{\mathrm{T}} \delta \mathbf{u}\, \mathrm{d}\Gamma \tag{3}$$

$$\delta f_i(\mathbf{x}_J)[u_i(\mathbf{x}_J) - g_i(\mathbf{x}_J)] = 0 \tag{4}$$

where $f_i(\mathbf{x}_J)$ and $u_i(\mathbf{x}_J)$ are the ith components of $\mathbf{f}(\mathbf{x}_J)$ and $\mathbf{u}(\mathbf{x}_J)$, respectively.

Consider an MLS approximation of the displacement at node J in the x_i direction $u_i(\mathbf{x}_J)$, denoted as [1–7]

$$u_i^h(\mathbf{x}_J) = \sum_{I=1}^{N} \boldsymbol{\Phi}_I(\mathbf{x}_J) d_I^i = \Phi_J^{i^{\mathrm{T}}} \mathbf{d} \tag{5}$$

where

$$\boldsymbol{\Phi}_J^{i^{\mathrm{T}}} = \begin{cases} \{\Phi_1(\mathbf{x}_J), 0, \Phi_2(\mathbf{x}_J), 0, \ldots, \Phi_N(\mathbf{x}_J), 0\}, & \text{when } i = 1 \\ \{0, \Phi_1(\mathbf{x}_J), 0, \Phi_2(\mathbf{x}_J), \ldots, 0, \Phi_N(\mathbf{x}_J)\}, & \text{when } i = 2 \end{cases}, \tag{6}$$

$$\mathbf{d} = \begin{Bmatrix} d_1^1 \\ d_1^2 \\ d_2^1 \\ d_2^2 \\ \vdots \\ d_N^1 \\ d_N^2 \end{Bmatrix} \tag{7}$$

is the vector of nodal parameters or generalized displacements, and N is the total number of nodal points in Ω. In Eq. (5), $\Phi_I(\mathbf{x})$ represents the meshless shape function associated with node I, defined as [1, 2, 4–7]

$$\Phi_I(\mathbf{x}) = \mathbf{p}^{\mathrm{T}}(\mathbf{x})\mathbf{A}^{-1}(\mathbf{x})\mathbf{C}_I(\mathbf{x}) \tag{8}$$

where

$$\mathbf{p}^{\mathrm{T}}(\mathbf{x}) = \{p_1(\mathbf{x}), \ldots, p_m(\mathbf{x})\} \tag{9}$$

is a vector of complete basis functions with $p_i(\mathbf{x}), i = 1, \ldots, m$ representing m monomials in $\mathbf{x}$,

$$\mathbf{A}(\mathbf{x}) = \mathbf{P}^{\mathrm{T}}\mathbf{W}\mathbf{P}\ , \tag{10}$$

$$\mathbf{C}_I(\mathbf{x}) = w_I(\mathbf{x})\mathbf{p}(\mathbf{x}_I)\ , \tag{11}$$

$$\mathbf{P} = \begin{bmatrix} \mathbf{p}^{\mathrm{T}}(\mathbf{x}_1) \\ \mathbf{p}^{\mathrm{T}}(\mathbf{x}_2) \\ \vdots \\ \mathbf{p}^{\mathrm{T}}(\mathbf{x}_N) \end{bmatrix} \in \mathscr{L}\left(\Re^N \times \Re^m\right)\ , \tag{12}$$

$$\mathbf{W} = \begin{bmatrix} w_1(\mathbf{x}) & 0 & \cdots & 0 \\ 0 & w_2(\mathbf{x}) & \cdots & 0 \\ \vdots & \vdots & \ddots & \vdots \\ 0 & 0 & \cdots & w_N(\mathbf{x}) \end{bmatrix} \in \mathscr{L}\left(\Re^N \times \Re^N\right) \tag{13}$$

and $w_I(\mathbf{x})$ is the weight function associated with node I such that $w_I(\mathbf{x}) > 0$ for all $\mathbf{x}$ in the support $\Omega_{\mathbf{x}} \subseteq \Omega$ of $w_I(\mathbf{x})$ and *zero* otherwise. A number of weight functions are available in the current literature [1, 2, 4]. A weight function developed by Rao and Rahman [1] was employed in this study, expressed as

$$w_I(\mathbf{x}) = \begin{cases} \dfrac{\left(1+\beta^2 \frac{z_I^2}{z_{mI}^2}\right)^{-\frac{1+\beta}{2}} - \left(1+\beta^2\right)^{-\frac{1+\beta}{2}}}{1-\left(1+\beta^2\right)^{-\frac{1+\beta}{2}}}, & z_I \le z_{mI} \\ 0, & z_I > z_{mI} \end{cases} \tag{14}$$

where β is a shape controlling parameter, $z_I = \|\mathbf{x} - \mathbf{x}_\mathbf{I}\|$ is the distance from a sample point $\mathbf{x}$ to a node $\mathbf{x}_I = \{x_{1I}, x_{2I}\}^{\mathrm{T}}$, and z_{mI} is the domain of influence of node I. To avoid any discontinuities in the shape functions due to the presence of cracks, a diffraction method [6] can be used to modify z_I in the weight function. According to this method, z_I is modified as [6]

$$z_I = \left(\frac{s_1 + s_2(\mathbf{x})}{s_0(\mathbf{x})}\right)^{\lambda} s_0(\mathbf{x}) \tag{15}$$

where $s_1 = \|\mathbf{x}_I - \mathbf{x}_c\|, s_2(\mathbf{x}) = \|\mathbf{x} - \mathbf{x}_c\|$, $s_0(\mathbf{x}) = \|\mathbf{x} - \mathbf{x}_I\|, \mathbf{x}_c = \{x_{1c}, x_{2c}\}^{\mathrm{T}}$ is a vector representing the coordinates of the crack tip, and $1 \le \lambda \le 2$ is a diffraction parameter.

Applying Eqs. (5–15), the discrete form of Eqs. (3) and (4) becomes [1, 2]

$$\begin{bmatrix} \mathbf{k} & \boldsymbol{\Phi}_J^i \\ \boldsymbol{\Phi}_j^{i^{\mathrm{T}}} & 0 \end{bmatrix} \begin{Bmatrix} \mathbf{d} \\ f_i(\mathbf{x}_J) \end{Bmatrix} = \begin{Bmatrix} \mathbf{f}^{\mathrm{ext}} \\ g_i(\mathbf{x}_J) \end{Bmatrix} \tag{16}$$

where

$$\mathbf{k} = \begin{bmatrix} \mathbf{k}_{11} & \mathbf{k}_{12} & \cdots & \mathbf{k}_{1N} \\ \mathbf{k}_{21} & \mathbf{k}_{22} & \cdots & \mathbf{k}_{2N} \\ \vdots & \vdots & \vdots & \vdots \\ \mathbf{k}_{N1} & \mathbf{k}_{N2} & \cdots & \mathbf{k}_{NN} \end{bmatrix} \in \mathscr{L}(\Re^{2N} \times \Re^{2N}) \tag{17}$$

is the stiffness matrix with

$$\mathbf{k}_{IJ} = \int_{\Omega} \mathbf{B}_I^{\mathrm{T}} \mathbf{D} \mathbf{B}_J\, \mathrm{d}\Omega \in \mathscr{L}(\Re^2 \times \Re^2)\ , \tag{18}$$

$$\mathbf{f}^{\mathrm{ext}} = \begin{Bmatrix} \mathbf{f}_1^{\mathrm{ext}} \\ \mathbf{f}_2^{\mathrm{ext}} \\ \vdots \\ \mathbf{f}_N^{\mathrm{ext}} \end{Bmatrix} \in \Re^{2N} \tag{19}$$

is the force vector with

$$\mathbf{f}_I^{\text{ext}} = \int_\Omega \Phi_I \mathbf{b}^{\mathrm{T}}\, \mathrm{d}\Omega + \int_{\Gamma_t} \Phi_I \bar{\mathbf{t}}^{\mathrm{T}} \mathrm{d}\Gamma \in \Re^2 \quad , \tag{20}$$

$$\mathbf{B}_I = \begin{bmatrix} \Phi_{I,1} & 0 \\ 0 & \Phi_{I,2} \\ \Phi_{I,2} & \Phi_{I,1} \end{bmatrix} \quad , \tag{21}$$

$$\mathbf{D} = \begin{cases} \frac{E}{1-v^2} \begin{bmatrix} 1 & v & 0 \\ v & 1 & 0 \\ 0 & 0 & \frac{1-v}{2} \end{bmatrix}, & \text{for plane stress} \\ \frac{E}{(1+v)(1-2v)} \begin{bmatrix} 1-v & v & 0 \\ v & 1-v & 0 \\ 0 & 0 & \frac{1-2v}{2} \end{bmatrix}, & \text{for plane strain} \end{cases} \tag{22}$$

is the elasticity matrix, E is the elastic modulus and v is Poisson's ratio. The partial derivative of $\Phi_I(\mathbf{x})$ with respect to x_i, required in Eq. (21), can be obtained as

$$\Phi_{I,i}(\mathbf{x}) = \mathbf{p}^{\mathrm{T}} \mathbf{A}^{-1} \mathbf{C}_{I,i} + \mathbf{p}^{\mathrm{T}} \mathbf{A}_{,i}^{-1} \mathbf{C}_I + \mathbf{p}_{,i}^{\mathrm{T}} \mathbf{A}^{-1} \mathbf{C}_I \tag{23}$$

where

$$\mathbf{C}_{I,i} = w_I \mathbf{p}_{,i}^{\mathrm{T}} + w_{I,i} \mathbf{p}^{\mathrm{T}} \quad , \tag{24}$$

$$\mathbf{A}_{,i}^{-1} = -\mathbf{A}^{-1} \mathbf{A}_{,i} \mathbf{A}^{-1} \quad , \tag{25}$$

$$\mathbf{A}_{,i} = \mathbf{P}_{,i}^{\mathrm{T}} \mathbf{W} \mathbf{P} + \mathbf{P}^{\mathrm{T}} \mathbf{W}_{,i} \mathbf{P} + \mathbf{P}^{\mathrm{T}} \mathbf{W} \mathbf{P}_{,i} \quad , \tag{26}$$

$$\mathbf{p}_{,i}^{\mathrm{T}} = \left\{ p_{1,i}, \ldots, p_{m,i} \right\} \quad , \tag{27}$$

$$w_{I,i}(\mathbf{x}) = \begin{cases} \dfrac{-\frac{1+\beta}{2}\left(1+\beta^2 \frac{z_I^2}{z_{mI}^2}\right)^{-\frac{3+\beta}{2}} \frac{2\beta^2 z_I}{z_{mI}^2} z_{I,i}}{1-(1+\beta^2)^{-\frac{1+\beta}{2}}}, & z_I \le 0 \\ 0, & z_I > 0 \end{cases} \tag{28}$$

and

$$z_{I,i} = \frac{x_i - x_{iI}}{z_I} \quad , \tag{29}$$

if $z_I = \|\mathbf{x} - \mathbf{x}_\mathbf{I}\|$. If $z_\mathbf{I}$ is modified according to Eq. (15), however,

$$z_{I,i} = \lambda \left(\frac{s_1 + s_2(\mathbf{x})}{s_0(\mathbf{x})} \right)^{\lambda - 1} \frac{(x_i - x_{ic})}{s_2(\mathbf{x})} + (1-\lambda) \left(\frac{s_1 + s_2(\mathbf{x})}{s_0(\mathbf{x})} \right)^{\lambda} \frac{(x_i - x_{iI})}{s_0(\mathbf{x})} \tag{30}$$

where

$$(\ )_{,i} = \frac{\partial (\ )}{\partial x_i} \quad .$$

Standard Gaussian quadratures can be used to evaluate the integrals for assembling the stiffness matrix and the force vector. In general, a 4×4 quadrature is adequate, except in cells surrounding a high stress gradient (e.g., near a crack tip) where an 8×8 quadrature is suggested.

2.2 Essential boundary conditions

The lack of Kronecker delta properties in the meshless shape functions Φ_I poses some difficulty in imposing essential boundary conditions in EFGM. As such, consider a transformation [1, 32, 33]

$$\hat{\mathbf{d}} = \Lambda \mathbf{d} \tag{31}$$

where

$$\hat{\mathbf{d}} = \begin{Bmatrix} u_1^h(\mathbf{x}_1) \\ u_2^h(\mathbf{x}_1) \\ u_1^h(\mathbf{x}_2) \\ u_2^h(\mathbf{x}_2) \\ \vdots \\ u_1^h(\mathbf{x}_N) \\ u_2^h(\mathbf{x}_N) \end{Bmatrix} \in \Re^{2N} \tag{32}$$

is the nodal displacement vector and

$$\Lambda = \begin{bmatrix} \Phi_1^{1^{\mathrm{T}}} \\ \Phi_1^{2^{\mathrm{T}}} \\ \Phi_2^{1^{\mathrm{T}}} \\ \Phi_2^{2^{\mathrm{T}}} \\ \vdots \\ \Phi_N^{1^{\mathrm{T}}} \\ \Phi_N^{2^{\mathrm{T}}} \end{bmatrix} \in \mathscr{L}(\Re^{2N} \times \Re^{2N}) \tag{33}$$

is the transformation matrix. Multiplying the first set of matrix equations in Eq. (16) by $\Lambda^{-\mathrm{T}}$ yields [1]

$$\begin{bmatrix} \hat{\mathbf{k}}_1^{\mathrm{T}} & 0 \\ \vdots & \vdots \\ \hat{\mathbf{k}}_{M-1}^{\mathrm{T}} & 0 \\ \hat{\mathbf{k}}_M^{\mathrm{T}} & 1 \\ \hat{\mathbf{k}}_{M+1}^{\mathrm{T}} & 0 \\ \vdots & \vdots \\ \hat{\mathbf{k}}_{2N}^{\mathrm{T}} & 0 \\ \Phi_J^{i^{\mathrm{T}}} & 0 \end{bmatrix} \begin{Bmatrix} \mathbf{d} \\ f_i(\mathbf{x}_J) \end{Bmatrix} = \begin{Bmatrix} \hat{f}_1^{\text{ext}} \\ \vdots \\ \hat{f}_{M-1}^{\text{ext}} \\ \hat{f}_M^{\text{ext}} \\ \hat{f}_{M+1}^{\text{ext}} \\ \vdots \\ \hat{f}_{2N}^{\text{ext}} \\ g_i(\mathbf{x}_J) \end{Bmatrix} \begin{matrix} \\ \\ \\ \leftarrow [2(J-1)+i]\text{th row} \\ \\ \\ \\ \leftarrow (2N+1)\text{th row} \end{matrix} \tag{34}$$

where $\hat{\mathbf{k}}_i^{\mathrm{T}}$ is a vector representing the ith row of

$$\hat{\mathbf{k}} = \begin{bmatrix} \hat{\mathbf{k}}_1^{\mathrm{T}} \\ \vdots \\ \hat{\mathbf{k}}_{2N}^{\mathrm{T}} \end{bmatrix} = \Lambda^{-\mathrm{T}} \mathbf{k} \quad , \tag{35}$$

$$\hat{\mathbf{f}}^{\text{ext}} = \Lambda^{-\mathrm{T}} \mathbf{f}^{\text{ext}} \quad , \tag{36}$$

and $M = (2J-1)+i$. Exchanging the Mth and the last row of Eq. (34) leads to

$$\begin{bmatrix} \hat{\mathbf{k}}_1^{\mathrm{T}} & 0 \\ \vdots & \vdots \\ \hat{\mathbf{k}}_{M-1}^{\mathrm{T}} & 0 \\ \Phi_J^{i^{\mathrm{T}}} & 0 \\ \hat{\mathbf{k}}_{M+1}^{\mathrm{T}} & 0 \\ \vdots & \vdots \\ \hat{\mathbf{k}}_{2N}^{\mathrm{T}} & 0 \\ \hat{\mathbf{k}}_M^{\mathrm{T}} & 1 \end{bmatrix} \begin{Bmatrix} \mathbf{d} \\ f_i(\mathbf{x}_J) \end{Bmatrix} = \begin{Bmatrix} \hat{f}_1^{\mathrm{ext}} \\ \vdots \\ \hat{f}_{M-1}^{\mathrm{ext}} \\ g_i(\mathbf{x}_J) \\ \hat{f}_{M+1}^{\mathrm{ext}} \\ \vdots \\ \hat{f}_{2N}^{\mathrm{ext}} \\ \hat{f}_M^{\mathrm{ext}} \end{Bmatrix} \begin{matrix} \\ \\ \\ \leftarrow [2(J-1)+i]\text{th row} \\ \\ \\ \\ \leftarrow (2N+1)\text{th row} \end{matrix} \tag{37}$$

which can then be uncoupled as

$$\mathbf{K}\mathbf{d} = \mathbf{F} \tag{38}$$

$$\hat{\mathbf{k}}_M^{\mathrm{T}}\mathbf{d} + f_i(\mathbf{x}_J) = \hat{f}_M^{\mathrm{ext}} \tag{39}$$

where

$$\mathbf{K} = \mathscr{m}_J^i\left(\hat{\mathbf{k}}\right) = \begin{bmatrix} \hat{\mathbf{k}}_1^{\mathrm{T}} \\ \vdots \\ \hat{\mathbf{k}}_{M-1}^{\mathrm{T}} \\ \Phi_J^{i^{\mathrm{T}}} \\ \hat{\mathbf{k}}_{M+1}^{\mathrm{T}} \\ \vdots \\ \vdots \\ \hat{\mathbf{k}}_{2N}^{\mathrm{T}} \end{bmatrix} \leftarrow [2(J-1)+i]\text{th row} \tag{40}$$

and

$$\mathbf{F} = \mathscr{m}_J^i\left(\hat{\mathbf{f}}^{\mathrm{ext}}\right) = \begin{Bmatrix} \hat{f}_1^{\mathrm{ext}} \\ \vdots \\ \hat{f}_{M-1}^{\mathrm{T}} \\ g_i(\mathbf{x}_J) \\ \hat{f}_{M+1}^{\mathrm{ext}} \\ \vdots \\ \vdots \\ \hat{f}_{2N}^{\mathrm{ext}} \end{Bmatrix} \leftarrow [2(J-1)+i]\text{th row} \tag{41}$$

are the modified stiffness matrix and force vectors, respectively.

In Eqs. (40) and (41), $\mathscr{m}_J^i$ is a matrix operator that replaces the $[2(J-1)+i]$th row of $\hat{\mathbf{k}}$ with $\Phi_J^{i^{\mathrm{T}}}$ and $\mathscr{n}_J^i$ is the matrix operator that replaces the $[2(J-1)+i]$th row of $\hat{\mathbf{f}}^{\mathrm{ext}}$ with $g_i(\mathbf{x}_J)$, resulting from the application of a single boundary constraint at node J. For multiple boundary constraints with N_c boundary conditions at nodes $J_1, J_2, \ldots, J_{N_c}$ applied in the directions $i_1, i_2, \ldots, i_{N_c}$, respectively, the resulting modified stiffness matrix and force vector are

$$\mathbf{K} = \prod_{l=1}^{N_c} \mathscr{m}_{J_l}^{i_l}(\hat{\mathbf{k}}) \tag{42}$$

and

$$\mathbf{F} = \prod_{l=1}^{N_c} \mathscr{m}_{J_l}^{i_l}(\hat{\mathbf{f}}^{\mathrm{ext}}) \ , \tag{43}$$

respectively. Using Eqs. (38), (42) and (43) the generalized displacement vector $\mathbf{d}$ can be solved efficiently without the application of any Lagrange multipliers [1].

2.3
The interaction integral and stress intensity factors

Let K_I and K_{II} denote the SIFs for mode-I and mode-II, respectively. These SIFs can be evaluated using an interaction integral [34] converted to a domain form [35, 36]. For example,

$$K_I = \frac{E'}{2} M^{(1,2)} \tag{44}$$

where

$$E' = \begin{cases} E, & \text{plane stress} \\ \dfrac{E}{1-\nu^2}, & \text{plane strain} \end{cases} \tag{45}$$

is the effective elastic modulus and $M^{(1,2)}$ is the interaction integral. Equation (44) includes the terms from the actual mixed mode state for the given boundary conditions (superscript 1) and the super-imposed near-tip mode I auxiliary state (superscript 2). In Eq. (44), $M^{(1,2)}$ is given by

$$M^{(1,2)} = \int_A \left[\sigma_{ij}^{(1)} \frac{\partial u_i^{(2)}}{\partial x_1} + \sigma_{ij}^{(2)} \frac{\partial u_i^{(1)}}{\partial x_1} - W^{(1,2)}\delta_{1j} \right] \frac{\partial q}{\partial x_j} \mathrm{d}A \tag{46}$$

where A is the area of the integral domain, σ_{ij} and u_i are the components of stress tensor and displacement vector, respectively, $W^{(1,2)}$ is the mutual strain energy from the two states and q is a weight function selected to have a value of *unity* at the crack tip, *zero* along the boundary of the domain and arbitrary elsewhere. Note that all quantities are evaluated with respect to the coordinate system with the crack tip as the origin. Following similar considerations K_{II} can be calculated from Eqs. (44–46), except the near-tip mode II state is selected as an auxiliary state while computing $M^{(1,2)}$.

3
Rates of fracture parameters

3.1
Virtual crack extension

In fracture analysis, the coordinates of all meshless nodes, or any other arbitrary point are measured using the crack tip as the origin, where the x_1 axis is oriented along the direction of the crack length and the x_2 axis is perpendicular to the crack length. When the crack tip is virtually perturbed by a small amount, say

$\delta\mathbf{a} = \{\delta a_1, \delta a_2\}^{\mathrm{T}}$ for which δa_1 and δa_2 represent the components of virtual crack extension in the x_1 and x_2 directions, the coordinates of all nodes and any arbitrary point, except the crack-tip node (the reference point), are virtually shifted in the opposite direction by the same amount, as shown in the Fig. 2. In general, $\delta\mathbf{a}$ has two components, δa_1 and δa_2, respectively measured along the crack-length direction and perpendicular to the crack-length direction. The variation of any arbitrary point $\mathbf{x}$ is then

$$\delta\mathbf{x} = \begin{cases} \delta\mathbf{x}_I, & \text{if } \mathbf{x} = \mathbf{x}_I \\ -\delta\mathbf{a}, & \text{otherwise} \end{cases} \tag{47}$$

where

$$\delta\mathbf{x}_I = \begin{cases} \mathbf{0}, & \text{if } I = \text{crack-tip node} \\ -\delta\mathbf{a}, & \text{if } I \neq \text{crack-tip node} \end{cases} \tag{48}$$

Note that Eq. (47) is valid only when the crack-tip node is virtually perturbed. If all nodes along the crack length are virtually perturbed proportionally to their distance from the crack tip, Eq. (47) can be generalized as

$$\delta\mathbf{x}_I = \begin{cases} -\bar{d}_c\delta\mathbf{a}, & \text{if } I \in \text{nodes along crack length} \\ -\delta\mathbf{a}, & \text{if } I \notin \text{nodes along crack length} \end{cases} \tag{49}$$

where $\bar{d}_c$ is the ratio of the distance between node I and the crack tip to the length of the crack.

3.2
Variations of basis, weight and shape functions

3.2.1
Variations of basis function and its derivatives

Once the variation $\delta\mathbf{x} = \{\delta x_1, \delta x_2\}^{\mathrm{T}}$ is determined, the resulting variation of the basis function can be obtained as

$$\delta\mathbf{p}^{\mathrm{T}}(\mathbf{x}) = \{\delta p_1(\mathbf{x}), \ldots, \delta p_m(\mathbf{x})\} \tag{50}$$

Likewise, the variation of the derivative of the basis function with respect to x_i can also be obtained as

$$\delta\mathbf{p}_{,i}^{\mathrm{T}}(\mathbf{x}) = \{\delta p_{1,i}(\mathbf{x}), \ldots, \delta p_{m,i}(\mathbf{x})\} \tag{51}$$

where $\delta p_{I,i}(\mathbf{x}) = \partial p_I(\mathbf{x})/\partial x_i$. The explicit expressions of $\delta\mathbf{p}^{\mathrm{T}}(\mathbf{x})$ and $\delta\mathbf{p}_{,i}^{\mathrm{T}}(\mathbf{x})$ for commonly used (linear and quadratic) and enriched (radially enriched and fully enriched) basis functions are given as follows:

Linear

$$\mathbf{p}^{\mathrm{T}}(\mathbf{x}) = \{1, x_1, x_2\} \tag{52}$$

$$\delta\mathbf{p}^{\mathrm{T}}(\mathbf{x}) = \{0, \delta x_1, \delta x_2\} \tag{53}$$

$$\delta\mathbf{p}_{,i}^{\mathrm{T}}(\mathbf{x}) = \{0, 0, 0\} \tag{54}$$

Quadratic

$$\mathbf{p}^{\mathrm{T}}(\mathbf{x}) = \{1, x_1, x_2, x_1^2, x_1x_2, x_2^2\} \tag{55}$$

$$\delta\mathbf{p}^{\mathrm{T}}(\mathbf{x}) = \{0, \delta x_1, \delta x_2, 2x_1\delta x_1, x_1\delta x_2 + x_2\delta x_1, 2x_2\delta x_2\} \tag{56}$$

$$\delta\mathbf{p}_{,i}^{\mathrm{T}}(\mathbf{x}) = \begin{cases} \{0, 0, 0, 2\delta x_1, \delta x_2, 0\}, & \text{when } i = 1 \\ \{0, 0, 0, 0, \delta x_1, 2\delta x_2\}, & \text{when } i = 2 \end{cases} \tag{57}$$

Radially enriched

$$\mathbf{p}^{\mathrm{T}}(\mathbf{x}) = \{1, x_1, x_2, \sqrt{r}\} \tag{58}$$

$$\delta\mathbf{p}^{\mathrm{T}}(\mathbf{x}) = \left\{0, \delta x_1, \delta x_2, \delta\sqrt{r}\right\} \tag{59}$$

$$\delta\mathbf{p}_{,i}^{\mathrm{T}}(\mathbf{x}) = \left\{0, 0, 0, \delta\left(\frac{x_i}{2r\sqrt{r}}\right)\right\} \tag{60}$$

Fully enriched

$$\mathbf{p}^{\mathrm{T}}(\mathbf{x}) = \left\{1, x_1, x_2, \sqrt{r}\cos\frac{\theta}{2}, \sqrt{r}\sin\frac{\theta}{2}, \sqrt{r}\sin\frac{\theta}{2}\sin\theta, \sqrt{r}\cos\frac{\theta}{2}\sin\theta\right\} \tag{61}$$

$$\delta\mathbf{p}^{\mathrm{T}}(\mathbf{x}) = \left\{0, \delta x_1, \delta x_2, \delta\left(\sqrt{r}\cos\frac{\theta}{2}\right), \delta\left(\sqrt{r}\sin\frac{\theta}{2}\right), \delta\left(\sqrt{r}\sin\frac{\theta}{2}\sin\theta\right), \delta\left(\sqrt{r}\cos\frac{\theta}{2}\sin\theta\right)\right\} \tag{62}$$

$$\delta\mathbf{p}_{,i}^{\mathrm{T}}(\mathbf{x}) = \begin{Bmatrix} 0 \\ 0 \\ 0 \\ \delta\left(\frac{x_i}{2r\sqrt{r}}\cos\frac{\theta}{2} - (-1)^{i+1}\frac{x_i}{2r\sqrt{r}}\sin\frac{\theta}{2}\right) \\ \delta\left(\frac{x_i}{2r\sqrt{r}}\sin\frac{\theta}{2} + (-1)^{i+1}\frac{x_i}{2r\sqrt{r}}\cos\frac{\theta}{2}\right) \\ \delta\left(\frac{x_i}{2r\sqrt{r}}\sin\frac{\theta}{2}\sin\theta + (-1)^{i+1}\frac{x_i}{2r\sqrt{r}}\cos\frac{\theta}{2}\sin\theta + (-1)^{i+1}\frac{x_i}{r\sqrt{r}}\sin\frac{\theta}{2}\cos\theta\right) \\ \delta\left(\frac{x_i}{2r\sqrt{r}}\cos\frac{\theta}{2}\sin\theta + (-1)^{i+1}\frac{x_i}{2r\sqrt{r}}\sin\frac{\theta}{2}\sin\theta + (-1)^{i+1}\frac{x_i}{r\sqrt{r}}\cos\frac{\theta}{2}\cos\theta\right) \end{Bmatrix} \tag{63}$$

where $x_1 = r\cos\theta$ and $x_2 = r\sin\theta$.

Detailed variations of dependent quantities in Eqs. (58–63) are given in Appendix A.

3.2.2
Variations of weight function and its derivatives

The variation of the weight function, defined by Eq. (14), can be obtained as

$$\delta w_I(\mathbf{x}) = \begin{cases} \dfrac{-\frac{1+\beta}{2}\left(1+\beta^2\frac{z_I^2}{z_{mI}^2}\right)^{-\frac{3+\beta}{2}}\frac{2\beta^2 z_I}{z_{mI}^2}\delta z_I}{1-(1+\beta^2)^{-\frac{1+\beta}{2}}}, & \delta z_I \leq 0 \\ 0, & \delta z_I > 0 \end{cases} \tag{64}$$

where

$$\delta z_I = \frac{1}{z_I}\left[(x_1 - x_{1I})\delta(x_1 - x_{1I}) + (x_2 - x_{2I})\delta(x_2 - x_{2I})\right] \tag{65}$$

if $z_I = \|\mathbf{x} - \mathbf{x}_\mathbf{I}\|$. However, if $z_\mathbf{I}$ is modified according to Eq. (15),

$$\delta z_I = \lambda\left(\frac{s_1+s_2(\mathbf{x})}{s_0(\mathbf{x})}\right)^{\lambda-1}\left(\frac{\delta s_1+\delta s_2(\mathbf{x})}{s_0(\mathbf{x})}-\frac{s_1+s_2(\mathbf{x})}{s_0^2(\mathbf{x})}\delta s_0(\mathbf{x})\right) \times s_0(\mathbf{x})+\left(\frac{s_1+s_2(\mathbf{x})}{s_0(\mathbf{x})}\right)^{\lambda}\delta s_0(\mathbf{x}) \tag{66}$$

where

$$\delta s_1 = \frac{1}{s_1}[(x_{1I}-x_{1c})\delta(x_{1I}-x_{1c})+(x_{2I}-x_{2c})\delta(x_{2I}-x_{2c})] \tag{67}$$

$$\delta s_2(\mathbf{x}) = \frac{1}{s_2(\mathbf{x})}[(x_1-x_{1c})\delta(x_1-x_{1c}) + (x_2-x_{2c})\delta(x_2-x_{2c})] \tag{68}$$

$$\delta s_0(\mathbf{x}) = \frac{1}{s_0(\mathbf{x})}[(x_1-x_{1I})\delta(x_1-x_{1I}) + (x_2-x_{2I})\delta(x_2-x_{2I})] \tag{69}$$

Similarly, the variation of the partial derivative of the weight function is given by

$$\delta w_{I,i} = \delta\left(\frac{\mathrm{d}w_I}{\mathrm{d}z_I}z_{I,i}\right) = \delta\left(\frac{\mathrm{d}w_I}{\mathrm{d}z_I}\right)z_{I,i}+\frac{\mathrm{d}w_I}{\mathrm{d}z_I}\delta z_{I,i} \tag{70}$$

where

$$\delta\left(\frac{\mathrm{d}w_I}{\mathrm{d}z_I}\right) = \begin{cases} \dfrac{\frac{1+\beta}{2}\left[\frac{3+\beta}{2}\left(1+\beta^2\frac{z_I^2}{z_{mI}^2}\right)^{-\frac{5+\beta}{2}}\frac{4\beta^4 z_I^2}{z_{mI}^4}-\left(1+\beta^2\frac{z_I^2}{z_{mI}^2}\right)^{-\frac{3+\beta}{2}}\frac{2\beta^2}{z_{mI}^2}\right]\delta z_I}{1-(1+\beta^2)^{-\frac{1+\beta}{2}}}, & \delta z_I \le 0 \\ 0, & \delta z_I > 0 \end{cases} \tag{71}$$

and

$$\delta z_{I,i} = \frac{\delta(x_i-x_{iI})}{z_I}-\frac{x_i-x_{iI}}{z_I^3}[(x_1-x_{1I})\delta(x_1-x_{1I}) + (x_2-x_{2I})\delta(x_2-x_{2I})] \tag{72}$$

if $z_I = \|\mathbf{x}-\mathbf{x}_\mathbf{I}\|$. However, if z_I is modified according to Eq. (15),

$$\begin{aligned}\delta z_{I,i} = {} & \lambda(\lambda-1)\left(\frac{s_1+s_2(\mathbf{x})}{s_0(\mathbf{x})}\right)^{\lambda-2} \times\left(\frac{\delta s_1+\delta s_2(\mathbf{x})}{s_0(\mathbf{x})}-\frac{s_1+s_2(\mathbf{x})}{s_0^2(\mathbf{x})}\delta s_0(\mathbf{x})\right)\frac{(x_i-x_{ic})}{s_2(\mathbf{x})} \\ & +\lambda\left(\frac{s_1+s_2(\mathbf{x})}{s_0(\mathbf{x})}\right)^{\lambda-1}\left(\frac{\delta(x_i-x_{ic})}{s_2(\mathbf{x})}-\frac{(x_i-x_{ic})\delta s_2(\mathbf{x})}{s_2^2(\mathbf{x})}\right) \\ & +\lambda(1-\lambda)\left(\frac{s_1+s_2(\mathbf{x})}{s_0(\mathbf{x})}\right)^{\lambda-1} \times\left(\frac{\delta s_1+\delta s_2(\mathbf{x})}{s_0(\mathbf{x})}-\frac{s_1+s_2(\mathbf{x})}{s_0^2(\mathbf{x})}\delta s_0(\mathbf{x})\right)\frac{(x_i-x_{iI})}{s_0(\mathbf{x})} \\ & +(1-\lambda)\left(\frac{s_1+s_2(\mathbf{x})}{s_0(\mathbf{x})}\right)^{\lambda}\left(\frac{\delta(x_i-x_{iI})}{s_0(\mathbf{x})}-\frac{(x_i-x_{iI})\delta s_0(\mathbf{x})}{s_0^2(\mathbf{x})}\right)\end{aligned} \tag{73}$$

Equations (64) and (71) assume that the domain of influence z_{mI} of node I is independent of an infinitesimally small virtual crack perturbation. This assumption is justified since any change in the domain of influence of a node is negligible when the virtual crack perturbation is small.

3.2.3 Variations of shape function and its derivatives

Using Eqs. (8) and (23), the variations of the shape function $\mathbf{\Phi}_I(\mathbf{x})$ and its partial derivative $\mathbf{\Phi}_{I,i}(\mathbf{x})$ are

$$\delta\mathbf{\Phi}_I = \delta\mathbf{p}^\mathrm{T}\mathbf{A}^{-1}\mathbf{C}_I+\mathbf{p}^\mathrm{T}\delta\mathbf{A}^{-1}\mathbf{C}_I+\mathbf{p}^\mathrm{T}\mathbf{A}^{-1}\delta\mathbf{C}_I \tag{74}$$

$$\begin{aligned}\delta\mathbf{\Phi}_{I,i} = {} & \delta\mathbf{p}_{,i}^\mathrm{T}\mathbf{A}^{-1}\mathbf{C}_I+\delta\mathbf{p}^\mathrm{T}\mathbf{A}_{,i}^{-1}\mathbf{C}_I+\delta\mathbf{p}^\mathrm{T}\mathbf{A}^{-1}\mathbf{C}_{I,i} \\ & +\mathbf{p}_{,i}^\mathrm{T}\delta\mathbf{A}^{-1}\mathbf{C}_I+\mathbf{p}^\mathrm{T}\delta\mathbf{A}_{,i}^{-1}\mathbf{C}_I+\mathbf{p}^\mathrm{T}\delta\mathbf{A}^{-1}\mathbf{C}_{I,i} \\ & +\mathbf{p}_{,i}^\mathrm{T}\mathbf{A}^{-1}\delta\mathbf{C}_I+\mathbf{p}^\mathrm{T}\mathbf{A}_{,i}^{-1}\delta\mathbf{C}_I+\mathbf{p}^\mathrm{T}\mathbf{A}^{-1}\delta\mathbf{C}_{I,i}\end{aligned} \tag{75}$$

where

$$\delta\mathbf{C}_I = \delta w_I(\mathbf{x})\mathbf{p}(\mathbf{x}_I)+w_I(\mathbf{x})\delta\mathbf{p}(\mathbf{x}_I) \tag{76}$$

$$\delta\mathbf{A} = \delta\mathbf{P}^\mathrm{T}\mathbf{W}\mathbf{P}+\mathbf{P}^\mathrm{T}\delta\mathbf{W}\mathbf{P}+\mathbf{P}^\mathrm{T}\mathbf{W}\delta\mathbf{P} \tag{77}$$

$$\delta\mathbf{A}^{-1} = -\mathbf{A}^{-1}\delta\mathbf{A}\mathbf{A}^{-1} \tag{78}$$

$$\begin{aligned}\delta\mathbf{C}_{I,i} = {} & \delta w_{I,i}(\mathbf{x})\mathbf{p}(\mathbf{x}_I)+w_{I,i}(\mathbf{x})\delta\mathbf{p}(\mathbf{x}_I) \\ & +\delta w_I(\mathbf{x})\mathbf{p}_{,i}(\mathbf{x}_I)+w_I(\mathbf{x})\delta\mathbf{p}_{,i}(\mathbf{x}_I)\end{aligned} \tag{79}$$

$$\delta\mathbf{A}_{,i}^{-1} = -\left[\delta\mathbf{A}^{-1}\mathbf{A}_{,i}\mathbf{A}^{-1}+\mathbf{A}^{-1}\delta\mathbf{A}_{,i}\mathbf{A}^{-1}+\mathbf{A}^{-1}\mathbf{A}_{,i}\delta\mathbf{A}^{-1}\right] \tag{80}$$

and

$$\begin{aligned}\delta\mathbf{A}_{,i} = {} & \delta\mathbf{P}_{,i}^\mathrm{T}\mathbf{W}\mathbf{P}+\mathbf{P}_{,i}^\mathrm{T}\delta\mathbf{W}\mathbf{P}+\mathbf{P}_{,i}^\mathrm{T}\mathbf{W}\delta\mathbf{P} \\ & +\delta\mathbf{P}^\mathrm{T}\mathbf{W}_{,i}\mathbf{P}+\mathbf{P}^\mathrm{T}\delta\mathbf{W}_{,i}\mathbf{P}+\mathbf{P}^\mathrm{T}\mathbf{W}_{,i}\delta\mathbf{P} \\ & +\delta\mathbf{P}^\mathrm{T}\mathbf{W}\mathbf{P}_{,i}+\mathbf{P}^\mathrm{T}\delta\mathbf{W}\mathbf{P}_{,i}+\mathbf{P}^\mathrm{T}\mathbf{W}\delta\mathbf{P}_{,i}\ .\end{aligned} \tag{81}$$

3.3 Rates of generalized displacements

Taking the variation on both sides of Eq. (38) yields,

$$\delta\mathbf{K}\mathbf{d}+\mathbf{K}\delta\mathbf{d} = \delta\mathbf{F} \tag{82}$$

where from Eqs. (42) and (43),

$$\delta\mathbf{K} = \prod_{l=1}^{N_c}\mathscr{m}_{J_l}^{i_l}\left(\delta\hat{\mathbf{k}}\right) \tag{83}$$

and

$$\delta\mathbf{F} = \prod_{l=1}^{N_c}\mathscr{m}_{J_l}^{i_l}\left(\delta\hat{\mathbf{f}}^{\mathrm{ext}}\right) \tag{84}$$

are the variations of modified stiffness matrix and force vector, respectively. The variation of the generalized displacement vector $\delta\mathbf{d}$ can then be solved from

$$\mathbf{K}\delta\mathbf{d} = \delta\mathbf{F}-\delta\mathbf{K}\mathbf{d} \tag{85}$$

Note, the solution of $\delta\mathbf{d}$ can be obtained efficiently, since the same set of linear equations as in Eq. (38), although with a different fictitious load, i.e., the right hand side of Eq. (85), is involved. Suppose the crack length is virtually perturbed by a small arbitrary value δa in the original

direction of the crack length, i.e., $\delta a_1 = \delta a$ and $\delta a_2 = 0$. The derivative of the generalized displacement **d** with respect to the crack length a can then be calculated as

$$\frac{\partial \mathbf{d}}{\partial a} \approx \frac{\delta \mathbf{d}}{\delta a} \tag{86}$$

Equation (86) was used for all numerical calculations presented in forthcoming sections.

Note that by assigning appropriate values of δa_1 and δa_2, similar expressions can be derived to calculate rates of **d** with respect to crack length extensions in any direction. For example, if the values of δa_1 and δa_2 are arbitrarily selected, then $\delta \mathbf{d}/\|\delta \mathbf{a}\|$ provides the rate of the generalized displacement with respect to the crack length extension at an angle $\tan^{-1}(\delta a_2/\delta a_1)$ with respect to the direction of the crack length, where $\|\delta \mathbf{a}\| = \sqrt{\delta a_1^2 + \delta a_2^2}$. This issue, however, was not explored in detail during the course of this study.

3.4 Rates of stress intensity factors

The derivative of the SIF K_I with respect to crack length a can be calculated from the derivatives of displacement, strain, and stress with respect to a at all meshless nodes. Differentiating both sides of Eq. (44) with respect to a yields

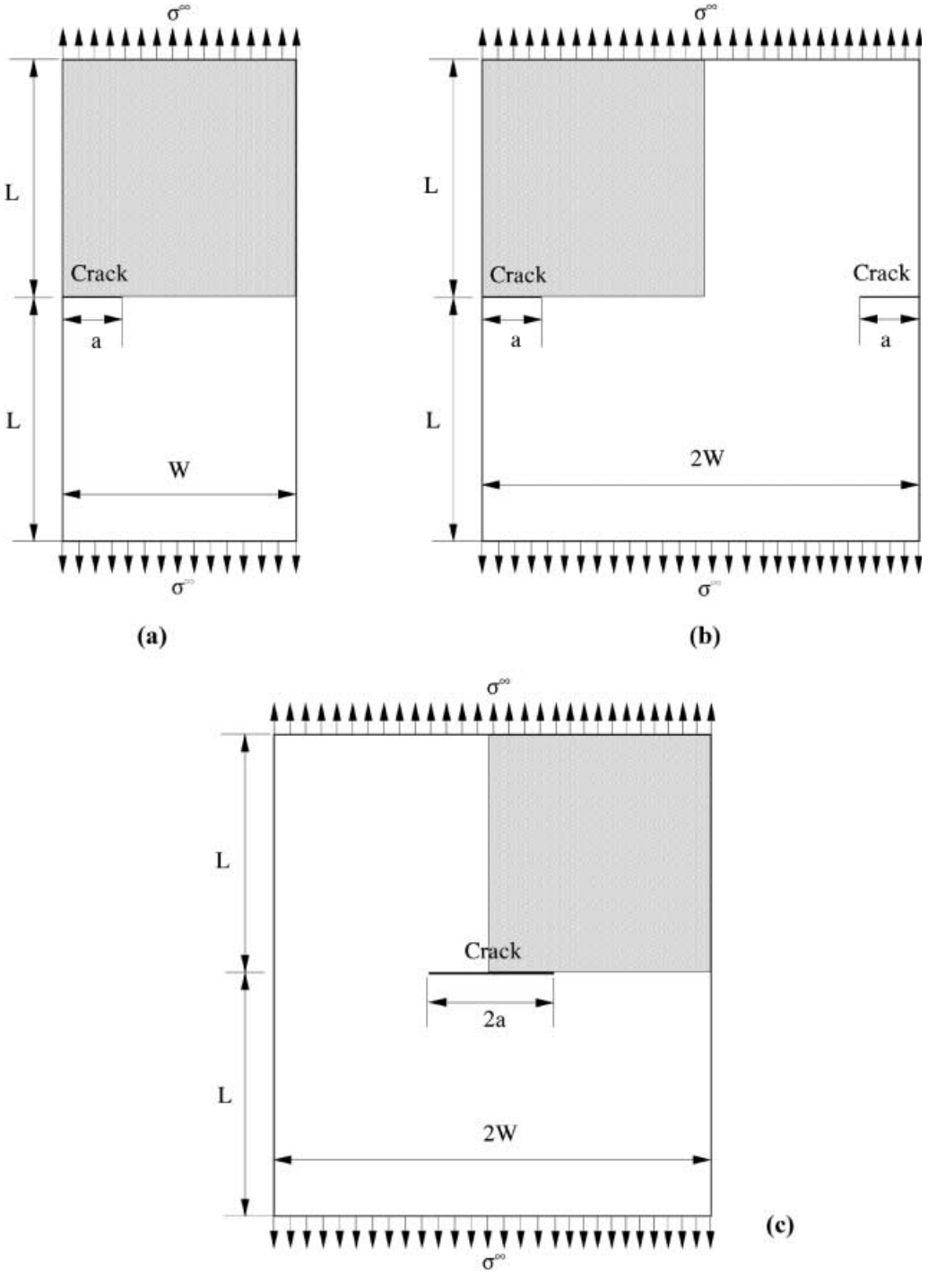

Fig. 3. Rectangular plates under far-field tension (mode I); **a** SE(T) specimen, **b** DE(T) specimen, and **c** M(T) specimen

$$\frac{\partial K_I}{\partial a} = \frac{E'}{2}\frac{\partial M^{(1,2)}}{\partial a} \tag{87}$$

where

$$\frac{\partial M^{(1,2)}}{\partial a} = \int_A \frac{\partial}{\partial a}\left[\sigma_{ij}^{(1)}\frac{\partial u_1^{(2)}}{\partial x_1} + \sigma_{ij}^{(2)}\frac{\partial u_i^{(1)}}{\partial x_1} - W^{(1,2)}\delta_{1j}\right]\frac{\partial q}{\partial x_j}\mathrm{d}A + \int_A \left[\sigma_{ij}^{(1)}\frac{\partial u_i^{(2)}}{\partial x_1} + \sigma_{ij}^{(2)}\frac{\partial u_i^{(1)}}{\partial x_1} - W^{(1,2)}\delta_{1j}\right]\frac{\partial}{\partial a}\left(\frac{\partial q}{\partial x_j}\right)\mathrm{d}A \tag{88}$$

In Eq. (88), the derivatives of stress components σ_{ij} with respect to a can be obtained using the derivatives of generalized displacements and the strain–displacement relation in conjunction with the stress–strain relation. Derivatives of the displacement components u_i with respect to a can be obtained using the derivatives of the generalized displacements and the shape function values of meshless nodes. Similarly, the derivative of K_{II} with respect to crack size a can also be computed from Eqs. (87) and (88), given that the near-tip mode II state is selected as the auxiliary state while computing $\partial M^{(1,2)}/\partial a$.

It should be noted that the sensitivity formulation developed in this study does not require any second-order variations of the stiffness matrix, unlike existing finite element methods [19, 24]. As a result, the proposed method is simpler than existing methods and can be easily extended to derive higher-order derivatives of stress-intensity factors.

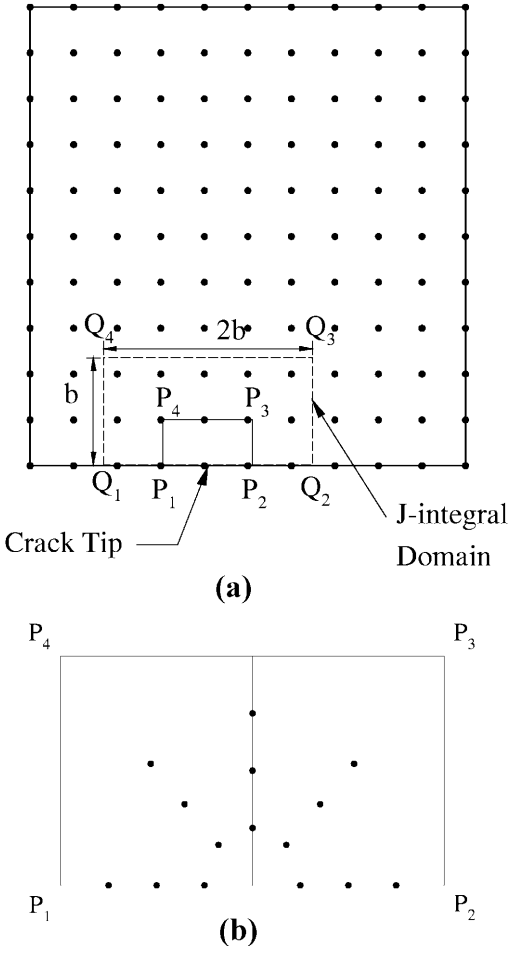

Fig. 4. Meshless discretizations; **a** uniformly spaced 121 nodes, **b** additional 15 nodes at crack-tip region

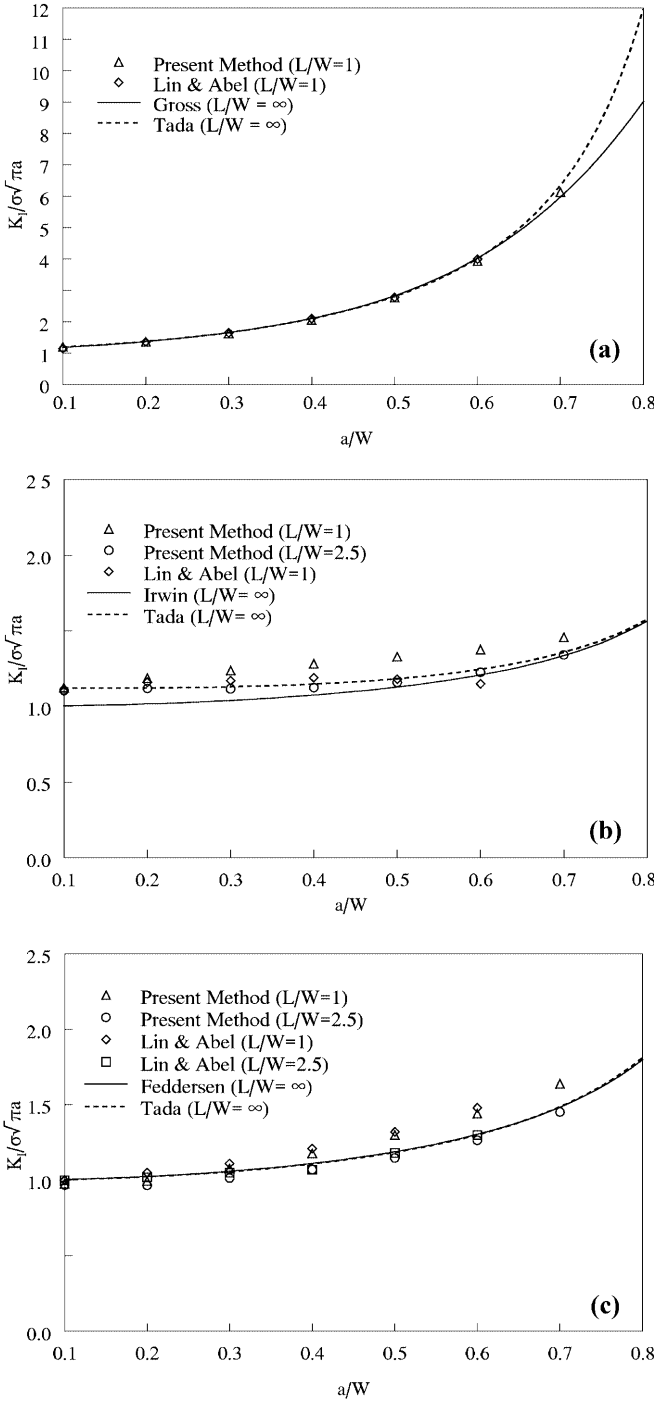

Fig. 5. SIF versus a/W ratio; **a** SE(T) specimen, **b** DE(T) specimen, and **c** M(T) specimen

4
Numerical examples

4.1
Example 1: Mode-I problems

Consider three rectangular plates illustrated in Fig. 3a–c, comprising single-edge tension [SE(T)], double-edge tension [DE(T)], and middle tension [M(T)] specimens, subjected to a far-field remote tensile stress σ^{∞} . For numerical analysis, values of $W = L = 1$ unit and $\sigma^{\infty} = 1$ unit were selected for all three plates. The crack length-to-width ratio (a/W) varied from 0.1 to 0.7. An elastic modulus of 20.7×10^6 units and Poisson's ratio of 0.30 were used.

Due to symmetry, meshless discretizations were performed for only half the plate for the SE(T) specimen, and a quarter of the plate for the DE(T) and M(T) specimens, as depicted by the shaded regions in Fig. 3a–c. A meshless discretization consisting of 121 uniformly spaced nodes was used for all three plates, as shown in Fig. 4a. However, for $a/W = 0.1$ and 0.2, 15 additional nodes were employed around the crack tip in the $P_1P_2P_3P_4$ region, as shown in the Fig. 4b. The domain of the plate in Fig. 4a was divided by 10×10 rectangular cells with corner points coincident with the 121 meshless nodes, solely for the purposes of numerical integration. The domain $Q_1Q_2Q_3Q_4$ of size $2b \times b$ with $b = \min\{a, (W - a)\}$ was used to calculate the interaction integral and its derivative, as shown in Fig. 4a. An 8×8 Gaussian integration scheme was employed over the background grid. A fully enriched basis function and $\beta = 3$ were used for meshless analysis. A plane stress condition was assumed for all three plates.

Figure 5a–c plot the normalized K_I versus a/W, as predicted by the meshless method for SE(T), DE(T), and M(T) plates, respectively. Also plotted are the corresponding finite element results [19] and other analytical K_I

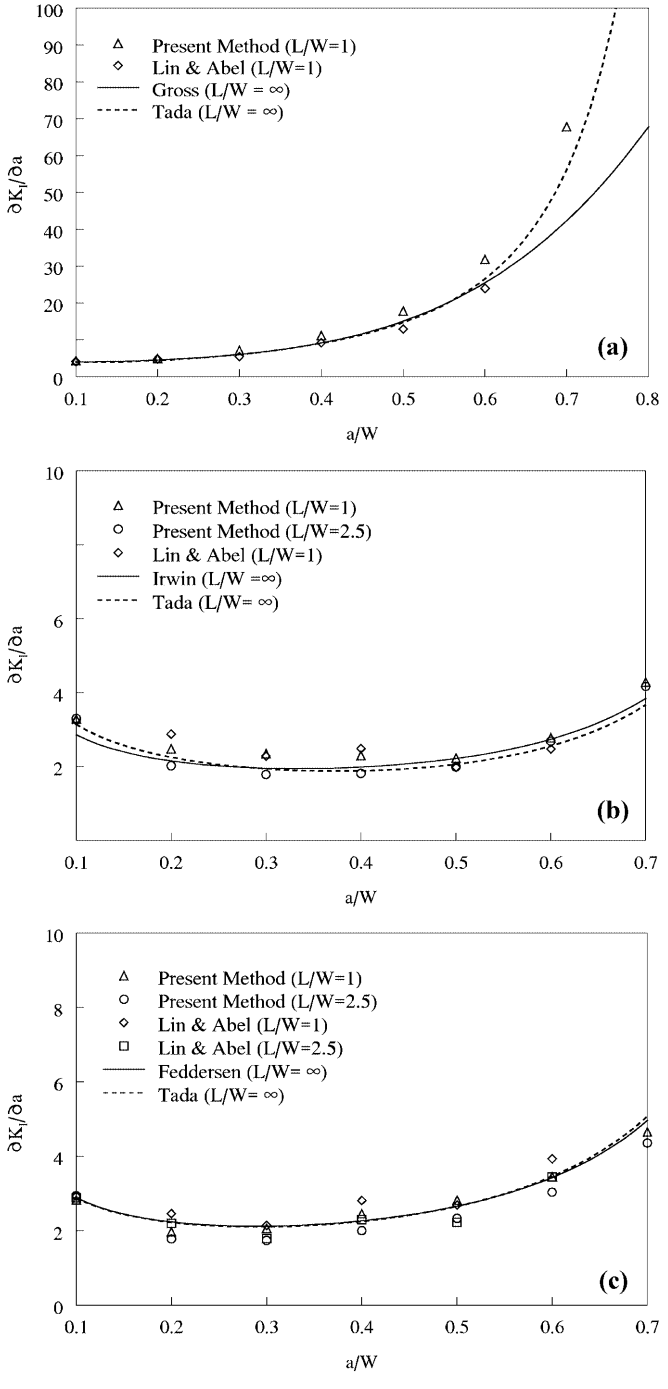

Fig. 6. Rates of SIF versus a/W ratio; **a** SE(T) specimen, **b** DE(T) specimen, and **c** M(T) specimen

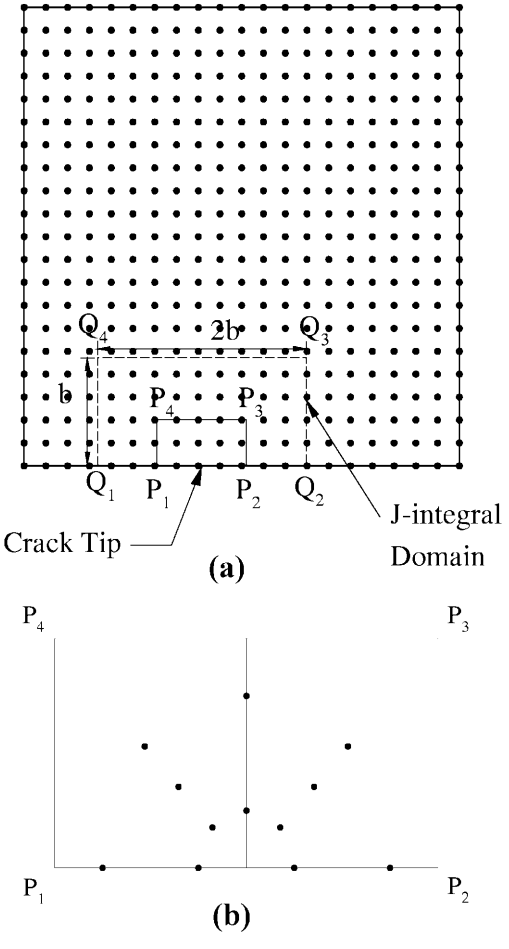

Fig. 7. Meshless discretizations; **a** uniformly spaced 441 nodes, **b** additional 12 nodes at crack-tip region

solutions available from current literature [37]. The meshless results compare very well with existing solutions.

Figure 6a–c show a similar comparison of $\partial K_I/\partial a$ as a function of a/W for all three plates. The plots in Fig. 6a–c include meshless results from this study, finite element results of Lin and Abel [19], and other solutions obtained by differentiating the analytical expressions of K_I as developed by Gross [37], Tada [37], Irwin [37], and Feddersen [37]. The $\partial K_I/\partial a$ results predicted using the proposed meshless method in conjunction with the virtual crack extension technique for the plate and crack geometry considered in this study match very well with the analytical and finite element solutions.

Note that the analytical expressions of K_I are available only for $L/W = \infty$. Hence, Figs. 5b, c and 6b, c also present respectively the results (K_I and $\partial K_I/\partial a$) of meshless analysis for the case $L/W = 2.5$. For this case, meshless analysis was performed for a quarter plate with dimensions $L = 2.5$ units, $W = 1$ unit and using 256 uniformly distributed meshless nodes.

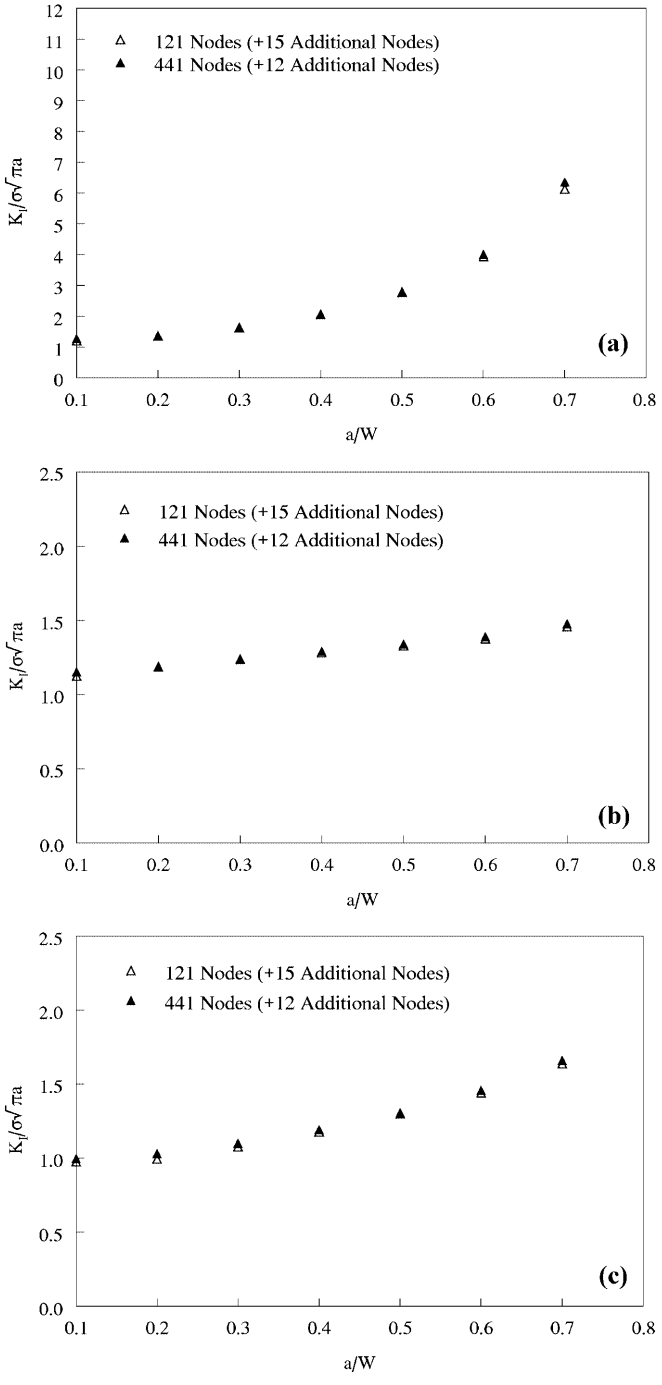

Fig. 8. Comparison of SIFs for various nodal refinements; **a** SE(T) specimen, **b** DE(T) specimen, and **c** M(T) specimen

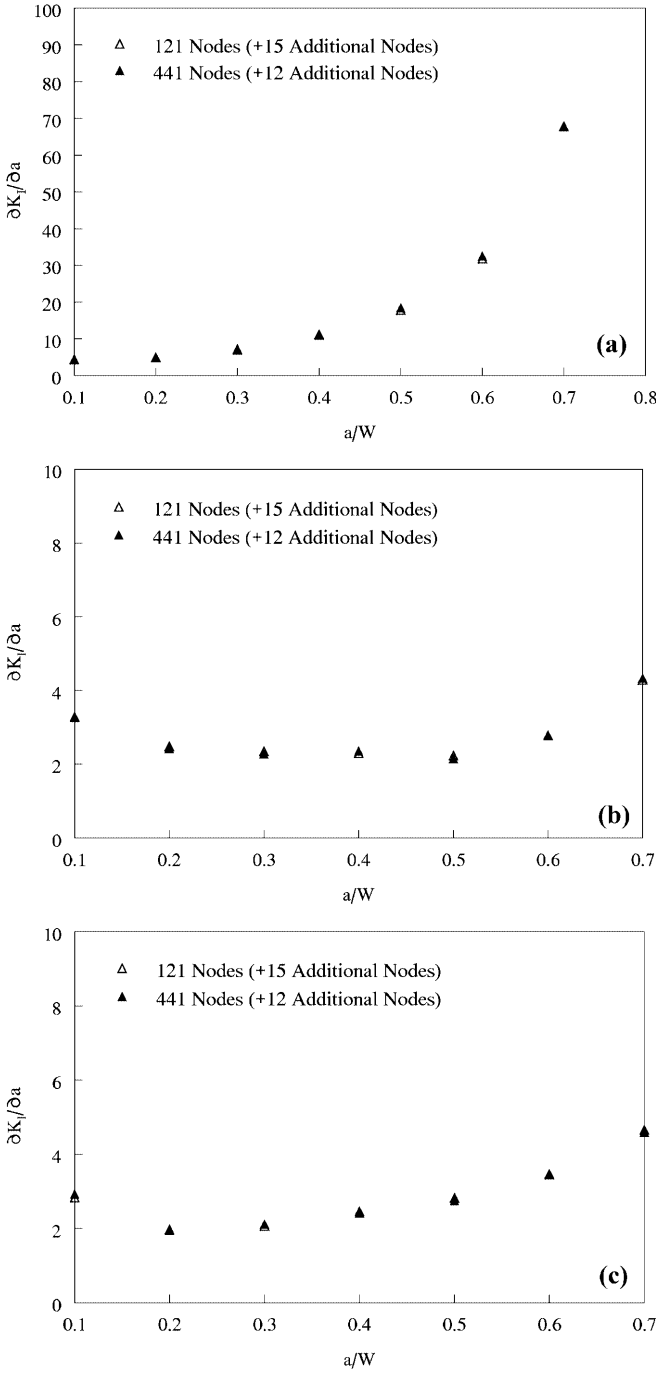

Fig. 9. Comparison of rates of SIFs for various nodal refinements; **a** SE(T) specimen, **b** DE(T) specimen, and **c** M(T) specimen

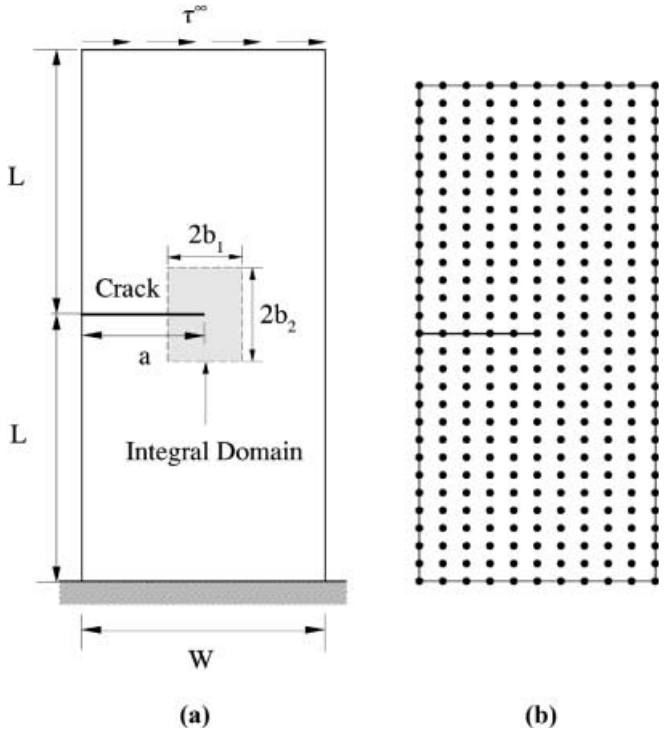

Fig. 10. Edged-cracked plate under far-field shear (mixed-mode); **a** geometry and loads, **b** meshless discretization for $a/W = 0.5$ (324 nodes)

Effect of nodal refinement and convergence of results for all three specimens with $L/W = 1$ were studied using a finer meshless discretization consisting of 441 uniformly spaced nodes, as shown in Fig. 7a. However, for $a/W = 0.1$ and 0.2, 12 additional nodes were employed around the crack tip in the $P_1P_2P_3P_4$ region, as shown in the Fig. 7b. Figure 8a–c compare the normalized K_I versus a/W plots for SE(T), DE(T), and M(T) plates, respectively, obtained by using two meshless discretizations of Figs. 4 and 7. Figure 9a–c show a similar comparison of $\partial K_I/\partial a$ as a function of a/W for all three plates. The agreement between the results of both discretizations is excellent.

4.2
Example 2: Mixed-mode problem

This mixed-mode example presents an edge-cracked plate, fixed at the bottom and subjected to a far-field shear stress $\tau^{\infty} = 1$ unit applied on the top, as shown in Fig. 10a. The dimensions of the plate were length $2L = 16$ units and width $W = 7$ units. The a/W ratio varied from 0.3 to 0.5. A domain of size $2b_1 \times 2b_2$ with $b_1 = b_2 = \min\{a, (W - a)\}$ was defined around the crack tip, as shown in Fig. 10a, to calculate the interaction integral and its derivative. Figure 10b shows the meshless discretization for $a/W = 0.5$ using 324 uniformly spaced nodes. No nodal refinements were employed. A background mesh with cell points coincident with meshless nodes was used. The elastic modulus and Poisson's ratio were 30×10^6 units and 0.25, respectively. A fully enriched basis function, $\beta = 3$, and $\lambda = 1$ were used for meshless analysis. A plane strain condition was assumed.

Tables 1 and 2 present, respectively, the predicted results for K_I and $\partial K_I/\partial a$ and K_{II} and $\partial K_{II}/\partial a$, for the edge-cracked plate under shear. In addition, both Tables 1 and 2 present finite-difference results for a 1% perturbation of crack length calculated in conjunction with a standard finite element method. The results in Tables 1 and 2 show that the proposed meshless method provides reasonably accurate estimates for $\partial K_I/\partial a$ and $\partial K_{II}/\partial a$ in comparison with the corresponding results of the finite-difference method. The maximum difference between the results of the proposed method and the finite-difference method is less than 7%.

5
Conclusions

A Galerkin-based meshfree method was developed for predicting the first-order derivatives of SIFs with respect to the crack size in a linear-elastic structure containing a single crack. The method comprises a meshless discretization of a cracked structure, a domain integral representation of the fracture integral parameter, and a sensitivity formulation in conjunction with a virtual crack extension technique. Unlike existing finite element meth-

Table 1. Mode-I SIF and its first-order derivative

a/W	SIF (K_I)			Rate of SIF ($\partial K_I/\partial a$)		
	Proposed method	FEM	Difference[a] (%)	Proposed method	Finite difference	Difference[a] (%)
0.3	19.71	19.82	−0.56	6.671	7.143	−6.6
0.4	25.54	25.68	−0.55	9.662	9.643	+0.2
0.5	33.61	34.09	−1.41	15.73	15.14	−3.9

[a] Difference = (FEM or Finite difference − Proposed method) × 100/FEM or finite difference

Table 2. Mode-II SIF and its first-order derivative

a/W	SIF (K_{II})			Rate of SIF ($\partial K_{II}/\partial a$)		
	Proposed method	FEM	Difference[a] (%)	Proposed method	Finite difference	Difference[a] (%)
0.3	2.50	2.46	1.63	1.447	1.476	−1.97
0.4	3.54	3.49	1.43	1.477	1.393	+6.03
0.5	4.61	4.54	1.54	1.476	1.486	−0.67

[a] Difference = (FEM or Finite difference − Proposed method) × 100/FEM or finite difference

ods, the proposed method does not require any second-order variation of the stiffness matrix. Hence, the proposed method is simpler than existing methods. The method developed herein can be extended to obtain higher-order derivatives of SIFs if desired. Several numerical examples based on mode-I and mixed-mode problems have been presented to illustrate the proposed method. The results show that the first-order derivatives of stress-intensity factors calculated using the proposed method methods for the structural and crack geometry considered in this study agree favorably with reference solutions obtained either analytically (mode I) or using finite-difference (mixed mode) method. For mixed-mode problems, the maximum difference between the results of proposed method and finite-difference method is less than seven percent. Since the rates of the SIFs are calculated analytically, the subsequent fracture reliability analysis can be performed efficiently and accurately.

Appendix A

The variations of dependent quantities in Eqs. (58–63) are

$$\delta\sqrt{r} = \frac{\delta r}{2\sqrt{r}} \quad , \tag{A.1}$$

$$\delta\left(\sqrt{r}\cos\frac{\theta}{2}\right) = \frac{1}{2\sqrt{r}}\delta r\cos\frac{\theta}{2} - \frac{\sqrt{r}}{2}\sin\frac{\theta}{2}\delta\theta \quad , \tag{A.2}$$

$$\delta\left(\sqrt{r}\sin\frac{\theta}{2}\right) = \frac{1}{2\sqrt{r}}\sin\frac{\theta}{2}\delta r + \frac{\sqrt{r}}{2}\cos\frac{\theta}{2}\delta\theta \quad , \tag{A.3}$$

$$\begin{aligned}\delta\left(\sqrt{r}\sin\frac{\theta}{2}\sin\,\theta\right) &= \frac{1}{2\sqrt{r}}\sin\,\frac{\theta}{2}\sin\theta\delta r \\ &\quad + \frac{\sqrt{r}}{2}\cos\frac{\theta}{2}\delta\theta\sin\theta \\ &\quad + \sqrt{r}\sin\,\frac{\theta}{2}\cos\theta\delta\theta \quad ,\end{aligned} \tag{A.4}$$

$$\begin{aligned}&\delta\left(\sqrt{r}\cos\frac{\theta}{2}\sin\,\theta\right) \\ &\quad = \frac{1}{2\sqrt{r}}\cos\frac{\theta}{2}\sin\,\theta\delta r - \frac{\sqrt{r}}{2}\sin\,\frac{\theta}{2}\delta\theta\sin\,\theta \\ &\qquad + \sqrt{r}\cos\,\frac{\theta}{2}\cos\,\theta\delta\theta \quad ,\end{aligned} \tag{A.5}$$

$$\begin{aligned}\delta\left(\frac{x_i}{r\sqrt{r}}\cos\frac{\theta}{2}\right) &= \frac{\delta x_i}{r\sqrt{r}}\cos\frac{\theta}{2} - \frac{3x_i}{2r^2\sqrt{r}}\cos\,\frac{\theta}{2}\delta r \\ &\quad - \frac{x_i}{2r\sqrt{r}}\sin\,\frac{\theta}{2}\delta\theta \quad ,\end{aligned} \tag{A.6}$$

$$\begin{aligned}\delta\left(\frac{x_i}{r\sqrt{r}}\sin\frac{\theta}{2}\right) &= \frac{\delta x_i}{r\sqrt{r}}\sin\frac{\theta}{2} - \frac{3x_i}{2r^2\sqrt{r}}\sin\,\frac{\theta}{2}\delta r \\ &\quad + \frac{x_i}{2r\sqrt{r}}\cos\,\frac{\theta}{2}\delta\theta \quad ,\end{aligned} \tag{A.7}$$

$$\begin{aligned}&\delta\left(\frac{x_i}{r\sqrt{r}}\sin\frac{\theta}{2}\sin\,\theta\right) \\ &\quad = \frac{\delta x_i}{r\sqrt{r}}\sin\frac{\theta}{2}\sin\,\theta - \frac{3x_i}{2r^2\sqrt{r}}\sin\frac{\theta}{2}\sin\,\theta\delta r \\ &\qquad + \frac{x_i}{2r\sqrt{r}}\cos\frac{\theta}{2}\sin\,\theta\delta\theta + \frac{x_i}{r\sqrt{r}}\sin\frac{\theta}{2}\cos\,\theta\delta\theta \quad ,\end{aligned} \tag{A.8}$$

$$\begin{aligned}&\delta\left(\frac{x_i}{r\sqrt{r}}\cos\frac{\theta}{2}\sin\,\theta\right) \\ &\quad = \frac{\delta x_i}{r\sqrt{r}}\cos\frac{\theta}{2}\sin\,\theta - \frac{3x_i}{2r^2\sqrt{r}}\cos\frac{\theta}{2}\sin\,\theta\delta r \\ &\qquad - \frac{x_i}{2r\sqrt{r}}\sin\frac{\theta}{2}\sin\,\theta\delta\theta + \frac{x_i}{r\sqrt{r}}\cos\frac{\theta}{2}\cos\,\theta\delta\theta \quad ,\end{aligned} \tag{A.9}$$

$$\begin{aligned}&\delta\left(\frac{x_i}{r\sqrt{r}}\sin\frac{\theta}{2}\cos\,\theta\right) \\ &\quad = \frac{\delta x_i}{r\sqrt{r}}\sin\frac{\theta}{2}\cos\,\theta - \frac{3x_i}{2r^2\sqrt{r}}\sin\frac{\theta}{2}\cos\,\theta\delta r \\ &\qquad + \frac{x_i}{2r\sqrt{r}}\cos\frac{\theta}{2}\cos\,\theta\delta\theta - \frac{x_i}{r\sqrt{r}}\sin\frac{\theta}{2}\sin\,\theta\delta\theta \quad ,\end{aligned} \tag{A.10}$$

and

$$\begin{aligned}&\delta\left(\frac{x_i}{r\sqrt{r}}\cos\frac{\theta}{2}\cos\,\theta\right) \\ &\quad = \frac{\delta x_i}{r\sqrt{r}}\cos\frac{\theta}{2}\cos\,\theta - \frac{3x_i}{2r^2\sqrt{r}}\cos\frac{\theta}{2}\cos\,\theta\delta r \\ &\qquad - \frac{x_i}{2r\sqrt{r}}\sin\frac{\theta}{2}\cos\,\theta\delta\theta - \frac{x_i}{r\sqrt{r}}\cos\frac{\theta}{2}\sin\,\theta\delta\theta \quad .\end{aligned} \tag{A.11}$$

In Eq. (A.1–A.11),

$$\delta r = \frac{x_1\delta x_1 + x_2\delta x_2}{\sqrt{x_1^2 + x_2^2}} \tag{A.12}$$

and

$$\delta\theta = \frac{x_1\delta x_2 - x_2\delta x_1}{x_1^2 + x_2^2} \quad . \tag{A.13}$$

References

1. **Rao BN, Rahman S** (2000) An efficient meshless method for fracture analysis of cracks. Comput. Mech. 26: 398–408
2. **Belytschko T, Lu YY, Gu L** (1995) Crack propagation by element-free Galerkin methods. Eng. Frac. Mech. 51(2): 295–315
3. **Sukumar N, Moran B, Belytschko T** (1998) The natural element method in solid mechanics. Int. J. Numer. Meth. Eng. 43: 839–887
4. **Kaljevic I, Saigal S** (1997) An improved element free Galerkin formulation. Int. J. Numer. Meth. Eng. 40: 2953–2974
5. **Belytschko T, Tabbara M** (1996) Dynamic fracture using element-free Galerkin methods. Int. J. Numer. Meth. Eng. 39: 923–938
6. **Fleming M, Chu YA, Moran B, Belytschko T, Lu YY, Gu L** (1997) Enriched element-free Galerkin methods for crack-tip fields. Int. J. Numer. Meth. Eng. 40: 1483–1504

7. **Belytschko T, Krongauz Y, Organ D, Fleming M, Krysl P** (1996) Meshless methods: an overview and recent developments. Comp. Meth. Appl. Mech. Eng. 139: 3–47
8. **Rahman S, Rao BN** (2001) A perturbation method for stochastic meshless analysis in elastostatics. Int. J. Numer. Meth. Eng. 50(8): 1969–1991
9. **Rahman S, Rao BN** (2001) An element-free Galerkin method for probabilistic mechanics and reliability. Int. J. Solids and Struct. 38(50–51): 9313–9330
10. **Rahman S, Xu H** (2001) A meshless method for solving boundary-value problems in stochastic mechanics. Proc. Monte Carlo Simulation, Monaco: 193-200
11. **Madsen HO, Krenk S, Lind NC** (1986) Methods of Structural Safety. Prentice-Hall, Inc., Englewood Cliffs, New Jersey
12. **Grigoriu M, Saif MTA, El-Borgi S, Ingraffea A** (1990) Mixed-mode fracture initiation and trajectory prediction under random stresses. Int. J. Frac. 45: 19–34
13. **Provan JW** (1987) Probabilistic Fracture Mechanics and Reliability. Martinus Nijhoff Publishers, Dordrecht, The Netherlands
14. **Besterfield GH, Liu WK, Lawrence MA, Belytschko T** (1991) Fatigue crack growth reliability by probabilistic finite elements. Comp. Meth. Appl. Mech. Eng. 86: 297–320
15. **Besterfield GH, Lawrence MA, Belytschko T** (1990) Brittle fracture reliability by probabilistic finite elements. ASCE J. Eng. Mech. 116(3): 642–659
16. **Rahman S** (1995) A stochastic model for elastic–plastic fracture analysis of circumferential through-wall-cracked pipes subject to bending. Eng. Frac. Mech. 52(2): 265–288
17. **Rahman S, Kim J-S** (2001) Probabilistic fracture mechanics for nonlinear structures. Int. J. Pres. Ves. Piping 78(4): 261–269
18. **Rahman S** (2001) Probabilistic fracture mechanics: *J*-estimation and finite element methods. Eng. Frac. Mech. 68: 107–125
19. **Lin SC, Abel J** (1988) Variational approach for a new direct-integration form of the virtual crack extension method. Int. J. Frac. 38: 217–235
20. **deLorenzi HG** (1982) On the energy release rate and the *J*-integral for 3-D crack configurations. Int. J. Frac. 19: 183–193
21. **deLorenzi HG** (1985) Energy release rate calculations by the finite element method. Eng. Frac. Mech. 21: 129–143
22. **Haber RB, Koh HM** (1985) Explicit expressions for energy release rates using virtual crack extensions. Int. J. Numer. Meth. Eng. 21: 301–315
23. **Barbero EJ, Reddy JN** (1990) The Jacobian derivative method for three-dimensional fracture mechanics. Commun. Appl. Numer. Meth. 6: 507–518
24. **Hwang CG, Wawrzynek PA, Tayebi AK, Ingraffea AR** (1998) On the virtual crack extension method for calculation of the rates of energy release rate. Eng. Frac. Mech. 59: 521–542
25. **Feijóo RA, Padra C, Saliba R, Taroco E, Vénere MJ** (2000) Shape sensitivity analysis for energy release rate evaluation and its application to the study of three-dimensional cracked bodies. Comp. Meth. Appl. Mech. Eng. 188(4): 649–664
26. **Haug EJ, Choi KK, Komkov V** (1986) Design Sensitivity Analysis of Structural Systems. Academic Press, New York, NY
27. **Taroco E** (2000) Shape sensitivity analysis in linear elastic fracture mechanics. Comp. Meth. Appl. Mech. Eng. 188(4): 697–712
28. **Chen G, Rahman S, Park YH** (2000) Shape sensitivity analysis in linear-elastic fracture mechanics. ASME J. Pres. Ves. Technol. Accepted (in press)
29. **Chen G, Rahman S, Park YH** (2001) Shape sensitivity and reliability analyses in linear-elastic fracture mechanics. Int. J. Frac. 112(3): 223–246
30. **Chen G, Rahman S, Park YH** (2001) Shape sensitivity analysis in mixed-mode fracture mechanics. Comput. Mech. 27(4): 282–291
31. **Rahman S, Rao BN** (2001) Probabilistic fracture mechanics by Galerkin meshless methods – Part II: reliability analysis. Comput. Mech. Parts I and II papers should be published in the same volume. You should have the information when you compile the volume
32. **Atluri SN, Kim HG, Cho JY** (1998) A local boundary integral equation (LBIE) method in computational mechanics, and a meshless discretization approach. Comput. Mech. 21: 223–235
33. **Chen JS, Wang HP** (2000) New boundary condition treatments in meshfree computation of contact problems. Comp. Meth. Appl. Mech. Eng. 187: 441–468
34. **Yau JF, Wang SS, Corten HT** (1980) A mixed-mode crack analysis of isotropic solids using conservation laws of elasticity. J. Appl. Mech. 47: 335–341
35. **Moran B, Shih F** (1987) Crack tip and associated domain integrals from momentum and energy balance. Eng. Frac. Mech. 27: 615–642
36. **Nikishkov GP, Atluri SN** (1987) Calculation of fracture mechanics parameters for an arbitrary 3-dimensional crack by the equivalent domain integral method. Int. J. Numer. Meth. Eng. 24: 1801–1821
37. **Tada H, Paris P, Irwin G** (1973) The Stress Analysis of Cracks Handbook. Del Research Corporation, Hellertown, Pennsylvania